Macroporous-Mesoporous Carbon Supported Ni Catalysts for the Conversion of Cellulose to Polyols

Bin Zhang,[a,c,d] Bin Chen,[b] Mark Douthwaite,[d] Qiang Liu,[a] Chao Zhang,*[a] Qifan Wu,[a] Ruhui Shi,[a] Peixuan Wu,[a] Fengyu Zhao,*[a] Graham Hutchings[d]

Carbon based materials are some of the most commonly studied catalysts for the conversion of cellulose to polyols. The catalytic performance of these materials, however, is typically limited by the access of the substrate to the active sites, which is governed by the poor solubility of cellulose in aqueous solutions. In an attempt to resolve this, we presented a novel hierarchical carbon material which was prepared by a dual-templating method. Transmission electron microscopy and porosity measurements confirmed that the resultant materials consisted of both spherical macropores and well-defined mesoporous channels. Additional characterisation of this material revealed that it has an exceptionally high surface area (>1110 m^2 / g) and a high concentration of acidic sites, which are considered to be crucial for the hydrolysis of cellulose. Ni nanoparticles were subsequently immobilised onto this material and some additional carbon supports. It was determined that the high surface area and porosity of the synthesised carbon material assisted with the dispersion of the Ni nanoparticles. This Ni catalyst was found to be highly efficient for the one-pot conversion of cellulose to polyols, which is proposed to be a consequence of both the high number of acid sites and excellent Ni dispersion. This approach to catalyst design, offers a novel method for the valorisation of cellulose.

Introduction

Lignocellulosic biomass is considered to be a promising alternative to fossil-based feedstocks for the production of liquid fuels and fine chemicals.[1, 2] Between 40 and 60 (weight %) of lignocellulose comprises of cellulose, which has led to increasing attention in the development of catalytic processes for its efficient valorisation.[3] Cellulose is a naturally occurring linear polymer consisting of between 100 to 20,000 units of D-anhydro-glucopyranose, which are linked by β-1,4-glycosidic bonds. Due to the complex hydrogen-bonding network between the OH groups in the structure, cellulose has a tough crystalline structure and as a result, is only sparingly soluble in water and difficult to hydrolyse. As such, developing processes which can efficiently dismantle the hydrogen-bonding network and facilitate the hydrolytic cleavage of the glycosidic bonds within the polymer chain, is considered to be key for its efficient conversion.

Numerous approaches have been reported for the conversion of cellulose.[4, 5] These include stoichiometric conversion with acids, bio-catalytic conversion over enzymes, ionic liquids and catalytic conversion over heterogeneous and homogeneous catalysts. Whilst the stoichiometric application of liquid acids offers a simple and generally efficient means of its conversion, such processes are often limited due to concerns regarding industrial acceptability and scalability. Indeed, similar concerns can also be made with regards to many of the other methods for its conversion. Heterogeneous systems developed on a lab-scale are typically easier to up-scale, which is of course desirable, especially given that lignocellulosic feedstocks are anticipated to displace conventional fossil-based feedstocks as the leading source of liquid fuels.[2]

Many carbon materials such as activated carbon (AC),[6] carbon black (CB),[5] carbon nanotubes (CNT),[7, 8] oxidised carbon (OC),[9] carbon nanofibers (CNF),[10] fullerenes (CNFu), graphene oxide (GRO), etc., have been studied as catalysts and support materials for the conversion of biomass.[11, 12] In a previous study, amorphous carbon materials bearing SO_3H, COOH and OH groups were found to be highly effective for the hydrolysis of cellulose into glucose.[13, 14] The derived activation barrier for the conversion of cellulose over these carbon materials was found to be significantly lower than that observed by sulfuric acid.[15] Despite this, the reaction rate was ultimately still found to be limited by the transfer resistance between solid catalysts and insoluble cellulose. Therefore, it can be postulated that advances in cellulose conversion by heterogeneous catalysts would benefit from the design of efficient multifunctional and hierarchical catalysts.

[a] State Key Laboratory of Electro-analytical Chemistry and Laboratory of Green Chemistry and Process, Changchun Institute of Applied Chemistry, Chinese Academy of Sciences, Changchun 130022, PR China

[b] State Key Laboratory of Rare Earth Resources Utilization and laboratory of Green Chemistry and Process, Changchun Institute of Applied Chemistry, Chinese Academy of Sciences, Changchun 130022, PR China

[c] University of Chinese Academy of Sciences, Beijing 100049, PR China

[d] Cardiff Catalysis Institute, School of Chemistry, Cardiff University, Cardiff, CF10 3AT, UK

* E-mail: czhang@ciac.ac.cn, zhaofy@ciac.ac.cn; Tel: +86 431 8526 2410, Fax: +86 431 8526 2410.

Initial studies into the conversion of cellulose by heterogeneous catalysts involved the application of mesoporous carbon CMK for the hydrolysis of cellulose. Fukuoka and co-workers suggested that the mesoporous nature of these materials was crucial for the hydrolysis of cellulose into soluble oligosaccharides.[16] In a subsequent study by Zhang and co-workers, it was revealed that tungsten carbide supported on various CMKs were highly effective for the conversion of cellulose to ethylene glycol.[17] Zhang and co-workers followed on from this by developing a series of M-Ni/CMK bimetallic catalysts which were also found to be highly active for this reaction.[18] In both cases, the high activity for cellulose hydrolysis was attributed to the mesoporous structure; the high surface areas and pore volumes of the support materials were postulated to promote the dispersion of the active metals. Indeed, in a previous publication of our own, we showed that the mesoporosity of a Ni/ZSM-5 catalyst promoted catalytic performance in the conversion cellulose to polyols.[19]

It is known that mesoporosity can contribute to the anchoring and dispersion of Ni nanoparticles due to channel confinement effect.[20] It is also known, that macroporous materials can assist in cellulose conversion, due to the accessibility of macromolecular substrates to internal acidic active sites. As such, we predict that the utilization of a dual-component material containing both meso- and macropores will eliminate the transfer limitations associated with using cellulose as a feedstock, and as a consequence, promote its hydrolysis. Herein, we have designed and synthesised a series of macro-mesoporous carbon catalysts (MMC), and loaded them with Ni nanoparticles to catalyse the conversion of cellulose to polyols.

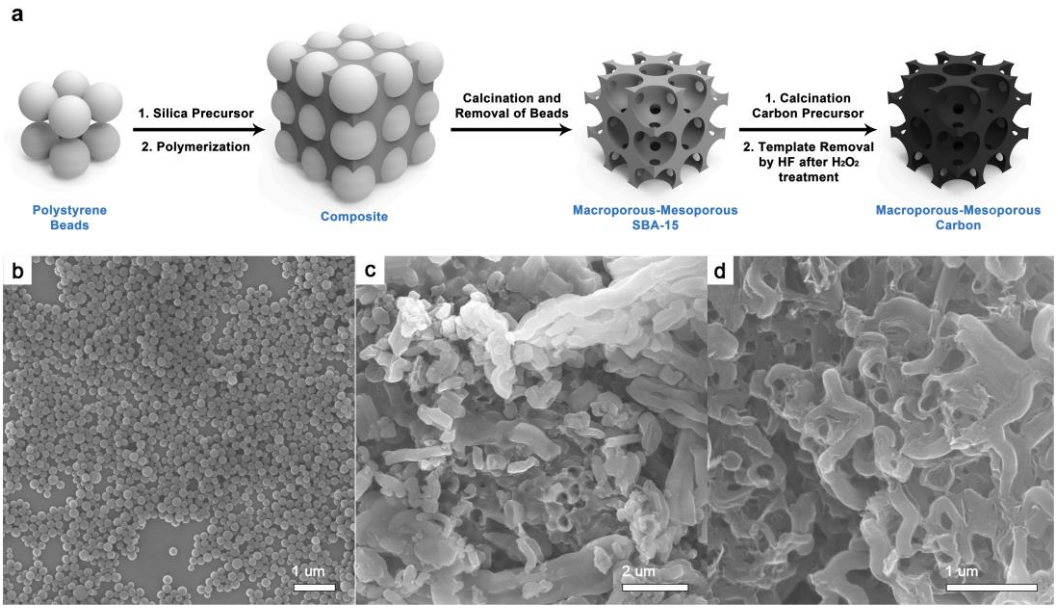

Figure 1. Illustration of the construction of MMC: a) using glucose as the carbon precursor and polymer as the hard template (a). The SEM images are shown here: (b) PS spheres (200 nm), (c) MM-SBA15-1, and (d) MMC materials.

Results

Screening of carbon support materials for the hydrogenolysis of cellulose over Ni nanoparticles

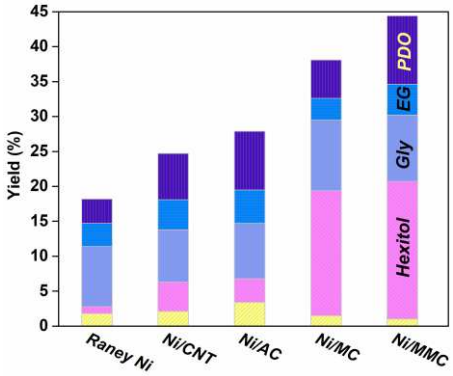

Figure 2. The bar chart of yield distribution of polyols over carbon catalysts in conversion of cellulose conversion at 240 °C under 4 MPa H_2 for 2.5 h. Herein, PDO: propanediol, EG: ethylene glycol, Gly: glycerol, and Hexitol: hexitol. Furthermore, CNT: carbon nanotubes, AC: active carbon, MC: mesoporous carbon, MMC: macro-mesoporous carbon. All loading of nickel metal is 12.5 wt%, except with the Raney Ni.

A macro-mesoporous carbon material (MMC) was synthesized by a dual-templating method, based on a modified nano-casting methodology. This was achieved by templating with PS spheres and *in-situ* formed SBA-15 from silica precursor TEOS. As illustrated in Figure 1, the initial MM-SBA15 composite was produced by mixing TEOS and PS spheres with the weight ratio of 6 (TEOS/PS) in the presence of pluronic P123 surfactants. This composite was calcined to remove the spheres and form macro-mesoporous SBA-15 (Figure 1c). This resultant compound was utilized as hard template and mixed with glucose, after removal of the template, which was finally generated to MMC-6 materials (Figure 1d). This material was then impregnated with $Ni(NO_3)_2{\cdot}6H_2O$ to produce the final Ni/MMC catalyst, the properties of which varied depending on the TEOS/PS ratio used in the dual-templating step. Previously, we investigated how the weight loading of Ni supported on ZSM-5 affected catalytic performance in the hydrogenolysis of cellulose.[21] The yield of polyols observed was comparable when Ni weight loadings of 17 % and 40 % were used. Interestingly, a notable reduction in the yield of polyols was observed when a Ni weight loading of 5 % was used. This observation was attributed to the fact that the first step hydrolysis of cellulose, is the rate-determining step in this cascade reaction and is catalyzed by the acidic nature of the support. As the rate of glucose hydrogenolysis is typically much faster, the difference in the product distribution only becomes discernable when low weight loadings of Ni are utilized. In this study, Ni catalysts with different loadings of Ni (12.5 %, 20 %, 25%) were tested

and found to give similar product distributions (Figure S2). Therefore, Ni weight loading of 12.5 % was used for all the catalysts in this study. Some additional carbon materials (carbon nanotubes, active carbon, mesoporous carbon) were also loaded with nickel metal using the same $Ni(NO_3)_2{\cdot}6H_2O$ impregnation procedure. Each of the supported Ni catalysts were subsequently assessed for their ability to catalyse the one-pot conversion of cellulose to polyols. The catalytic performance and distribution of the polyols (propanediol, ethylene glycol, glycerol, and hexitol) formed over each catalyst is displayed in Figure 2. The Ni nanoparticles supported on the microporous active carbon and mesoscale nanotubes gave polyol yields equal to approximately 25%. A slight increase in polyol yield was achieved over the Ni supported on a macropore-free carbon support (37%). The highest polyol yield however, was formed over the Ni/MMC-6 catalyst (45%), which was almost twice than the yield over AC and CNT supports.

The morphologies and structure of this catalyst Ni/MMC-6 are displayed in Figure 3. A large quantity of well-ordered mesoporous channels (~4 nm) can be observed in Figure 3a-b. Inside these mesoscale channels, a high concentration of Ni nanoparticles are confined, whose diameter is focusing on approximately 2~4 nm, as shown on the same line. These nanoparticles appear to be fairly uniformly dispersed over the mesoporous support, as shown in Figure 3c, which was evidenced by the broader diffraction peak of nickel metal (43˚) in the XRD pattern of this MMC material (Figure 5). In Figure 3d–f, the spherical macropores in the MMC material are also clearly visible (d-f), and larger Ni nanoparticles (3~7 nm) dispersed over their surface.

Alignment of catalytic performance of MMC catalysts with their physical properties

In order to investigate how the meso- and macro-porosity of the MMC supports influenced the performance of this catalyst in this reaction, two additional MMC materials with differing meso- and micro-porosity were subsequently synthesised and immobilised with Ni nanoparticles using the same method described previously. This was achieved by varying the ratio of TEOS to PS spheres in the preparation (18:1 and 1:1).

The catalytic performance of these MMC materials is shown in Figure 4. The hydrogenolysis of the cellulose over the Ni/MMC-6 catalyst led to the highest yield of polyols and interestingly, all of the Ni/MCC catalysts gave higher polyol yields than all the other that were assessed.

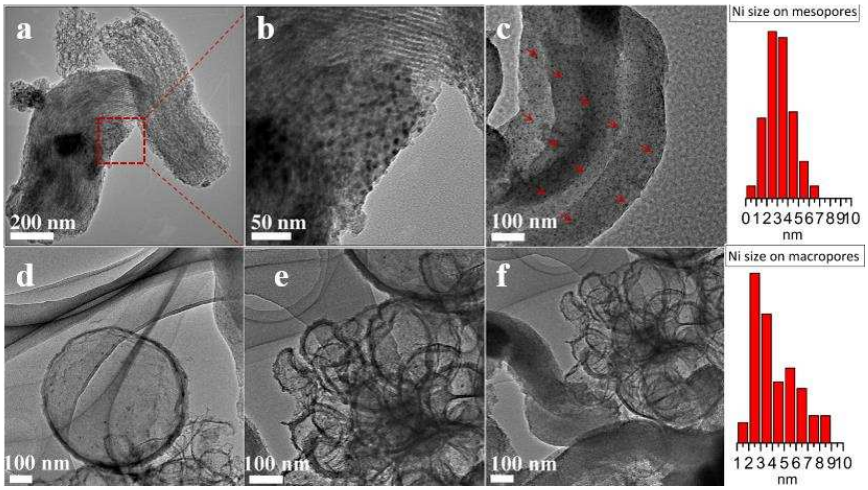

Figure 3. TEM images of the Ni/MMC-6 catalyst. The well-ordered and parallel mesoporous channels (a-c), inside them a large quantity of Ni nanoparticles (2~4 nm) are confined (b), and homogeneously and uniformly dispersed over the mesoporous surface (c). Moreover, a lot of spherical macropores and much larger Ni nanoparticles (3~7 nm) dispersed over the macroporous surface (d-f).

Discussion

1. A key area identified for improving polyol yields

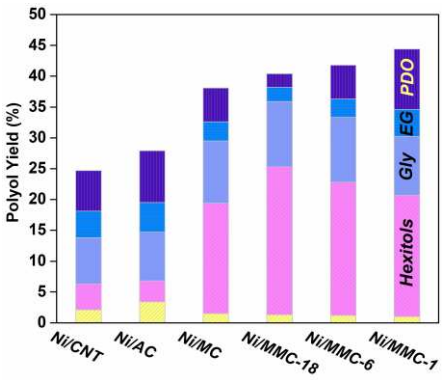

Figure 4. The total polyol productivity of the carbon catalysts. Here, the value (18, 6, 1) represents the actual weight ratio of the weight ratio of mesopore to macropore templates during the templating stage of the preparation, denoted as the indicator of relative proportion of mesopore to macropore.

The one-pot catalytic hydrogenolysis of cellulose at high temperatures (>230 °C) is a complicated process which requires a cascade of reactions to take place in order to obtain the polyol products.[22] This cascade first requires the depolymerization of insoluble cellulose into soluble oligosaccharide, which undergo subsequent hydrolysis into glucose monomers and can then finally undergo hydrogenation into hexitol.[23] Sequential C-C cleavages can then lead to the production of propanediol (PDO), glycerol (Gly), ethylene glycol (EG) and many other desirable compounds.[24, 25] There are however, a lot of additional side reactions from intermediates (glucose, hexitol and other polyols) which make promoting the reaction selectivity to these products more challenging.[22] These side reactions include the dehydration of glucose, aqueous phase reforming[26] and water-gas shift reaction.[27] The desirable reaction pathway is displayed in Scheme 1 and shows that the conversion of cellulose into polyols can be divided into two fundamental steps: the hydrolysis of cellulose to glucose units, and the subsequent hydrogenolysis of these intermediates into polyols.[28] The first step is considered to be rate-determining and as discussed previously, is likely to be due to the poor solubility of cellulose in an aqueous medium. The rate of hydrolysis is therefore likely to be dependent on the diffusion and adsorption of

cellulose to and from the active sites of the catalyst. If this is the case, then it is logical to suggest that the rate of this reaction is likely to be improved by increasing the surface areas and pore volumes of the catalyst support, to grant increased access of the substrate to internal acidic active sites.[19] It was also postulated that improving these physical properties may also assist with the dispersion of Ni on the surface of the support, which would be beneficial for the sequential hydrogenolysis step. This provided the motivation for the synthesis of the hierarchical carbon materials.

Scheme 1. The pathway of production of polyols from direct conversion of cellulose (hydrolysis and hydrogenolysis). Herein, polyols contain hexitol, glycerol, propanediol and ethylene glycol.

2. Synthesis and characterisation of MMC catalysts

In order to identify how the meso- and macroporous properties in the MMC catalyst effected the catalytic performance in this reaction, three MMC materials were synthesized which consisted of dramatically different quantities of both pores. As discussed previously, this was achieved by adjusting the ratio of TEOS to PS spheres (18, 6 and 1) used in the templating stage of the preparation. The SEM images corresponding to each of these three materials are illustrated in Figure S3. A reduced number of spherical macropores can be observed in the MMC-18 material, which is likely due to the reduced quantity of PS spheres used in the templating stage. In contrary, the MMC-1 material appears to have a much larger proportion of macropores. Each of these materials was subsequently immobilized with nickel and the corresponding XRD patterns are displayed in Figure 5a. The microporous catalyst (Ni/AC), gives a sharp diffraction peak at 2θ = 43°, which is characteristic of metallic Ni. In contrary, over the hierarchical catalysts (Ni/MMC, Ni/MC, Ni/CNT), this peak is significantly broader, suggesting that the dispersion of Ni over these catalysts is higher. This observation is further evidenced by results obtained from TEM and H_2-TPD experiments (Figure S5). These catalysts then were tested in order to determine how these structural modifications effected the catalytic performance. The results of these experiments are displayed in Figure 4, and more specific reaction data is also displayed in Figure S1. From the testing data, it is evident that the Ni/MMC-6 gives the highest yield of polyols, highlighting that the quantity of macropores in the MMC support influences the performance of the catalyst. N_2 adsorption-desorption experiments were subsequently conducted in order to derive pore size distributions, BET surface areas and pore volumes of the catalysts. The corresponding N_2-sorbtion curves and pore size distributions are displayed in Figure 5. The sorption isotherms corresponding to the hierarchical carbon catalysts (Ni/MMC), independent of the proportion of meso/macropore, show a typical IV-type isotherm, which was also observed with the Ni/CNT catalyst. In all cases, these materials exhibited a H3 hysterisis, which is characteristic of regular cylindrical pores and is in agreement with the well-ordered mesoscale channels observed in corresponding TEM images. In contrary, a I -type isotherm, characteristic of microporous materials, was observed for the Ni/AC catalyst. The total surface areas and pore volumes determined for the MMC materials were substantially higher than that determined for AC and CNT materials. The surface areas of all the MMC catalysts were found to be in excess of 1110 $m^2 \cdot g^{-1}$, while the surface areas determined for the AC and CNT which substantially lower (~250 $m^2 \cdot g^{-1}$). In addition to the surface areas, the pore volumes of all the MMC catalysts obtained from N_2 sorption, were also found to be much higher than that observed in the Ni/AC and Ni/CNT catalysts. Additional quantitative data regarding the corresponding pore volumes of each catalyst are provided in Table S1. The AC and CNT catalysts were found to have the lowest micropore volume, while the Ni/MMC-6 catalyst had the highest one. The macropore and mesopore volumes in these catalysts also followed the same trend. Given that the yield of polyols formed in the reaction aligned with the pore volumes, it can be concluded that the larger pore volumes allow for greater accessibility of the substrate to the catalytic active sites (both acidic sites and metal sites).

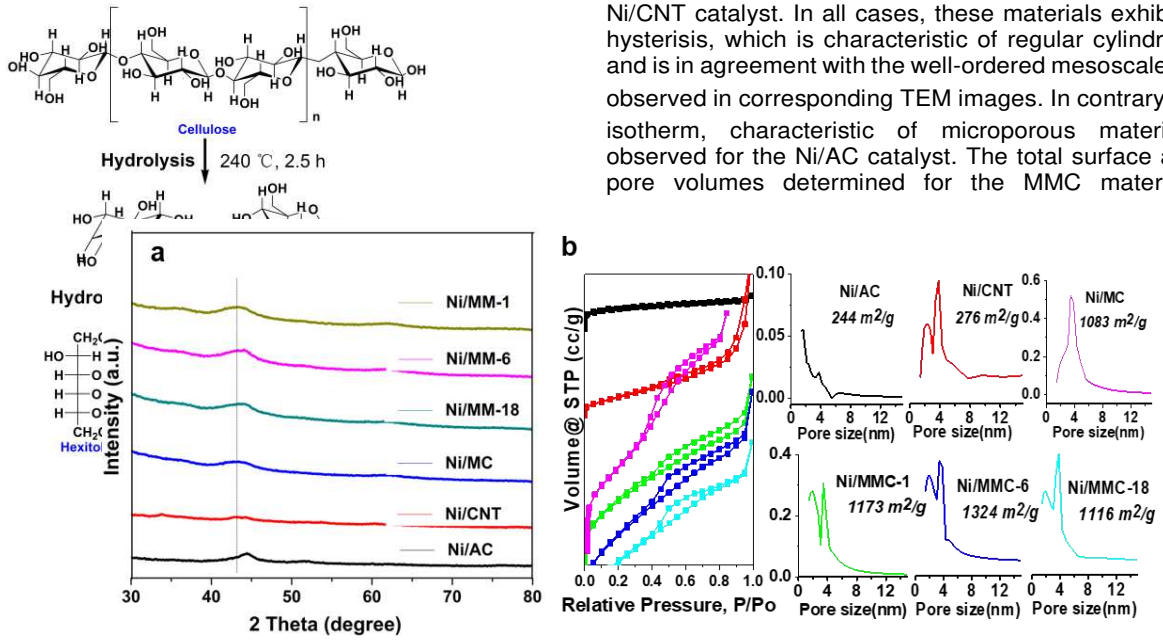

Figure 5. (a) XRD patterns of carbon-supporting nickel catalysts. Vertical black line represents the diffraction peak of nickel metal. The active carbon has a sharp peak and each of others show a broader peak. (b) Physic structural properties of carbon catalysts: N_2-sorption curve, distribution of pore size (nm) and BET surface areas ($m^2 \cdot g^{-1}$).

3. Origin of the improved activity from the hierarchical structure of MMC

In addition to enhancements in surface area and pore volume, it was also important to determine whether these materials exhibited any additional properties which may contribute to the formation of polyols from cellulose.[29] As discussed previously, it is known that acid sites on the carbon support facilitate the hydrolysis of both cellulose and glucose.[30] In order to investigate the nature of the acid sites on each of the catalysts, some NH_3-TPD experiments were conducted (Figure S4). Using this method however, It was difficult to accurately quantity and compare the acidity between the catalysts as in some cases, the presence of stronger acid sites (NH_3 desorption peak ≥ 500 °C) were concealed by the partial decomposition of the carbon support material. In previous

studies, Boehm titrations have been used to characterise the total surface acidity of carbon materials by quantifying surface bound oxygenated groups such as –COOH, Ph-OH, -OH, esters and lactones. For this reason, the oxygenated functional groups on the surface of the catalysts in this study were probed combining this methodology with the differential potentiometric titrator. The electrochemical titration curves corresponding to these experiments are displayed in Figure 6.

Two significant events are observed in the electronic potential curves for each of the catalysts tested. The total acidity was subsequently calculated by subtracting the remaining quantity of the titrant ($NaOC_2H_5$) left at the end of the experiment, as illustrated in Figure 6. The total acidity of the catalysts tested followed the trend CNT< AC< MMC-6, which aligns directly with their exhibited catalytic performance, as displayed in Figure 2.

In this reaction, high yields of polyols are dependent on both the quantity of acid sites and Ni sites available. The acid sites predominantly determine the rate of the reaction as they are responsible for the initial hydrolysis of cellulose. The presence of too many acid or Ni sites can however lead to sequential C-C or C-O cleavages in the polyols or reaction intermediates. In contrary, if the quantity of these sites is insufficient, it can lead to inefficient hydrolysis/hydrogenolysis in the reaction.[19, 21] For this reason, an optimum proportion of both sites is required in order to achieve high polyol yields. We therefore propose that the novel hierarchical carbon materials have a dual function for promoting the conversion of cellulose to polyols; these materials provide a greater number of accessible acid sites and also increase the dispersion of Ni on the surface of carbon support. To establish whether Ni was leached from the catalysts during a standard reaction, the solutions of the

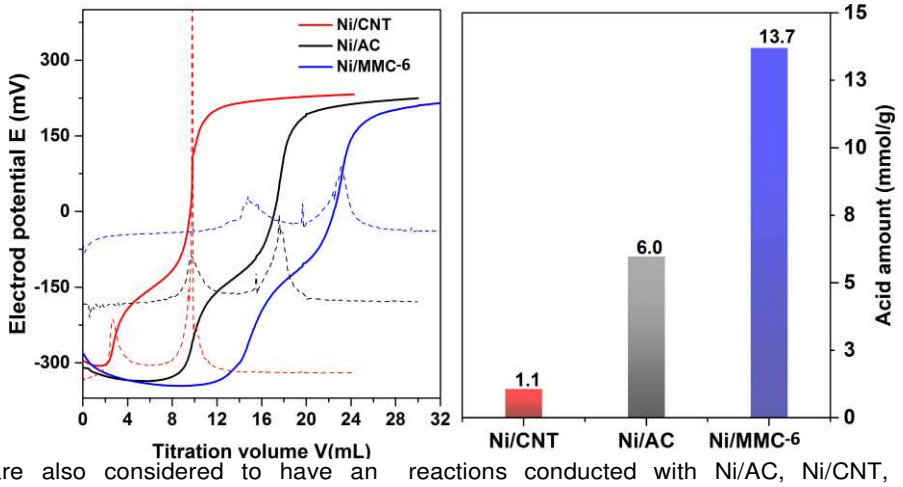

The Ni nanoparticles are also considered to have an important impact on hydrogenolysis of glucose intermediate into polyols. Based on H_2-TPD profiles of the above-mentioned catalysts (Figure S5), Ni nanoparticles are likely to exhibit a better dispersion on hierarchical MMC and MC materials than on the conventional carbon materials (CNT, AC). We can attribute this to the larger hydrogen desorption peak in low temperature (<100 °C).

reactions conducted with Ni/AC, Ni/CNT, and Ni/MMC-6 catalysts were analysed by ICP. It was determined that 0.7 %, 1.2 % and 0.5 % Ni leached from these catalysts respectively. Given that the lowest Ni leaching was observed with the Ni/MMC-6 catalyst, it suggests that this hierarchical support material is helpful to immobilize Ni nanoparticles and suppress the leaching of Ni species, compared to conventional benchmark carbon support.

Figure 6. The total surface acidity of catalysts determined by Boehm titration with HCl solution. The titration curve of electrode potential as a function of titration volume was shown in the left side figure. The first jump point (V1) is attributed to the precise consumption of excess $NaOC_2H_5$, while the second jump point (V2) is attributed to the amount of NaOH which was produced by hydrolysis of other $NaOC_2H_5$ in HCl aqueous solution. The total acid amount of catalysts was calculated by the total amount minus the surplus amount of $NaOC_2H_5$ (V1+V2), as shown in the right bar chart. (More details see Table S2)

Conclusion

To conclude, a series of hierarchical-structured carbon materials were synthesised by a dual-templating methodology. By carefully controlling the ratio of macropores to mesopores, the total acid concentration of the catalyst can reach 13.6 mmol/g, which is twice than that observed with the conventional activated carbon support and 13 times than that observed with the carbon nanotubes used in this study. The optimized Ni/MMC catalyst was used to convert cellulose into polyols and was found to be highly effective for the production of polyols. The presence of both macropores and mesopores increases the number of accessible acidic sites and promotes the dispersion and confinement of Ni nanoparticles. This study not only provides useful knowledge for the synthesis of carbon-based acid catalysts, but also provides a novel approach to catalyst design for applications in biomass conversion.

Experiment

1. Materials

Styrene (99%, TCI Co., Ltd.), divinylbenzene (80%, Aladdin Co., Ltd.), All gases (N_2, H_2, Air, Ar and 5% H_2/Ar gas, >99.999%, Changchun Juyang Gas Co., Ltd, China), potassium persulfate (99%, Xilong Chemical Co., Ltd, China), P123 (*M*w = 5,800, Sigma-Aldrich Co., Ltd.), TEOS (SiO_2 >28.5%, Beijing Yili Fine Chemicals Co., Ltd, China), glucose (98%, Aladdin Co., Ltd), $Ni(NO_3)_2{\cdot}6H_2O$ (A.R., Sinopharm Chemical Reagent Co., Ltd, China).

2. Catalyst preparation

Synthesis of polystyrene spheres

Polystyrene (PS) spheres were prepared by following a method proposed by Vaudreuil et al.[31-33] For this, styrene (25 mL) and divinylbenzene (4.75 mL) were first washed with NaOH (100 mL, 0.1 M) and subsequently with H_2O (200 mL) to remove any polymerization inhibitors (impurities). This washing step was repeated 3 times. The mixture of styrene and divinylbenzene was then transferred to a 500 mL flask and stirred in water (240 mL) at 70 °C under an Ar atmosphere for 1 h. Potassium persulfate (0.083 g) was subsequently added to initiate the polymerization of styrene. After stirring for 15 h,

the resultant solution was filtered and then washed three times with ethanol (240 mL). The PS spheres were collected and vacuum dried at 80 °C for a further 24 h. Their shape was regularly spherical and their size was 197 nm, which was shown in TEM images (Figure 1).

Synthesis of the macro-mesoporous SBA-15 silica

The macro-mesoporous SBA-15 silicas (MM-SBA15) were prepared *via* a dual-templating route.[34] For this, pluronic P123 surfactants and the PS spheres were used to template the macroporosity and mesoporosity of the resulting material respectively. In a typical preparation, P123 (3.0 g) was dissolved in de-ionized water (22.5 mL) and HCl (90 mL, 2 mol/L) on stirring at 35 °C. The desired amount of PS spheres was added to the solution, according to the weight ratio of TEOS:PS (X = 18,6 or 1) and a fixed amount of TEOS (6.9 mL). The solution was then exposed to an ultrasonic treatment for 1 h and subsequently stirred for an additional 1 h. Following that, TEOS (6.9 mL) was added to the solution, which was maintained at 35 °C for a further 24 h with constant stirring. The mixture was subsequently aged for 24 h at 80 °C and the resultant solid product was filtered, washed three times with de-ionized water (240 mL), and calcined under static air at 550 °C for 6 h (temperature ramp = 0.5 °C·min^{-1}). The final solid is denoted as MM-SBA15-X (X = 18,6 or 1).

Synthesis of the macro-mesoporous carbon

The macro-mesoporous carbon (MMC-X) was prepared by a modified nano-casting method, which utilized glucose as the carbon precursor and the newly synthetic MM-SBA15-X silicas as the hard template.[35] In a typical preparation, MM-SBA15-X silica (1.71 g) was impregnated with 1.2 g of glucose in the presence of concentrated H_2SO_4 (3 drops) and de-ionized water (4.5 g). The resulting material was dried at 24 °C for an initial 10 h and then 80 ℃ for 6 h, and finally 150 °C for an additional 6 h. A modified version of the above impregnation procedure was then conducted, this time however, glucose (0.75 g), concentrated H_2SO_4 (2 drops) and de-ionized water (4.5 g) were used in the impregnation step. After this was completed, the resulting material was heated at 80 °C for 6 h and 150 °C for an additional 6 h. The final solid was subsequently carbonized at 900 °C for 6 h (temperature ramp = 5 °C·min^{-1}) under an Ar atmosphere. The material was then washed in a solution of H_2O_2 (30% wt in H_2O, 25 mL) at 50°C for 5 h and finally washed in a solution containing HF (10 wt.% in H_2O, 25mL) for a further 16 h, to ensure that the complete removal of silica template., After filtration, washing with ethanol (200 mL), and vacuum drying at 80°C for 24 h, the final MMC-X material was obtained. Thermogravimetric analysis (TGA) was carried out to ensure that no silica residues remained in the material.

Preparation of the 12.5 wt.% Ni/MMC catalysts

The supported Ni catalysts were prepared by an incipient wetness impregnation method.[36] The surface-oxidized support materials (MC and MMC-X) were immersed in a precursor solution containing $Ni(NO_3)_2{\cdot}6H_2O$ (A.R., Sinopharm Chemical Reagent Co., Ltd, China) in de-ionized water (10 mL). This was followed by vacuum drying at 120 °C for 4 h. All catalysts were subsequently reduced under a flowing 5% H_2/Ar environment at 300 °C for 2 h (temperature ramp = 5°C·min^{-1}). In this study, the Ni loading (12.5 wt.% Ni) was calculated and determined by testing the weight of NiO in the calcined carbon catalyst (15.9% NiO). This result was subsequently confirmed by ICP method.

3. Catalyst characterization

Powder X-ray diffraction (XRD) patterns were obtained using a Bruker D8 Advance X-ray powder diffraction instrument with a Cu-Ka radiation (k=0.154 nm, 40 kV and 10 mA,) in the 2θ range of 20–80° with a scan speed of 1° min^{-1}. Transmission electron microscopy (TEM) images were taken using a field emission JEOL JEM-2010 instrument at 200 kV. The metal loading of each catalyst was collected by ICP-OES on a Thermo iCAP 6300 spectrometer. Scanning electron microscopy (SEM) images were collected on a Philips XL-30 field emission scanning electron microscope. BET surface areas were determined by N_2 adsorption-desorption experiments (BET) with a Micromeritics ASAP 2020 apparatus. H_2 temperature-programmed reduction and desorption experiments (H_2-TPR/H_2-TPD) were conducted on a Micromeritics Autochem II 2920 chemisorption instrument. NH_3 temperature-programmed desorption (NH_3-TPD) experiments were conducted on a Tianjin XQ TP-5080 chemisorption instrument attached with a thermal conductivity detector (TCD).

In a typical H_2-TPR experiment, catalyst (50 mg) was pre-treated in air at 150 °C for 1 h to remove physically adsorbed H_2O and other impurities. After cooling to room temperature, the sample was flushed for an additional 0.5 h and then heated to 850 °C at a rate of 10 °C·min^{-1} in a flowing 5% H_2/Ar (50 cm^3·min^{-1}). In a typical H_2-TPD experiment, catalyst (50 mg) was pre-reduced for 1 h at an appropriate temperature in a flowing 5% H_2/Ar. After cooling to room temperature, the sample was flushed for an additional 0.5 h and then heated to 850 °C at a heating rate of 10 °C·min^{-1} in a flowing Ar (50 cm^3·min^{-1}). In a typical NH_3-TPD experiment, catalyst (50 mg) was pre-treated in air at 150°C for 1 h. After cooling to room temperature, the sample was flushed with 0.2% NH_3/He for 30 min and then in He for an additional 1h. The desorption of NH_3 was then monitored as the temperature of the sample was heated to 850 °C (heating at 10 °C min^{-1}) in a flowing Ar (50 cm^3 min^{-1}).

Boehm titrations were conducted in order to identify the oxygen-containing acidic functional groups on surface of carbon materials.[37] In this method (a) $NaHCO_3$ determines the acid amount of –COOH; (b) Na_2CO_3 determines the amount of both –COOH/lactone groups; (c) NaOH determines the amount of –COOH/Ph–OH/lactone groups; (d) $NaOC_2H_5$ was used to determine the total acidic amount of –COOH, Ph–OH, lactone and carboxyl groups. Herein, strongly alkaline $NaOC_2H_5$ was applied to test the total surface acidity of carbon catalysts, combined on an electrochemical titration apparatus. Incipiently, catalyst (50 mg) was dispersed in an ethanol solution (25 mL), and subsequently the given amount of $NaOC_2H_5$ was added into this solution under stirring for 10 minutes. Finally, the HCl standard solution titrated back the solution on an electrochemical apparatus.

4. Catalytic reaction

Before any testing was carried out, microcrystalline cellulose (relative crystallinity of about 74.6%, Alfa Aesar) was first dried at 70 °C for 24 h. In a standard reaction,[38] catalyst (0.05 g) was reduced *in-situ* under H_2 at 400 °C for 2 h at a heating rate of 5 °C min^{-1}. The catalyst was then immediately transferred to a 50 mL Teflon-lined stainless-steel autoclave. To this, microcrystalline cellulose (0.1 g) and water (5 mL) were added and the autoclave was sealed. The reactor was then purged with H_2 (2-3 MPa) three times and finally charged with H_2 (4 MPa). The reactor was subsequently heated to 240 °C without stirring. Upon reaching the desired reaction temperature, the reactor was stirred at 1300 rpm. Once the reaction was complete, the reactor was cooled down to room temperature by immersing the sealed reactor in icy water. The autoclave was opened and the solid was separated from the liquid phase solution by centrifugation. The remaining solid was dried at 110°C for 16 h to determine the degree of cellulose conversion and the liquid phase sample was analysed by GC-MS and HPLC.

5. Product analysis

The liquid phase products formed in the reaction were initially identified by GC-MS (Agilent 5975/6890N) attached with a HP-5 column (30 m×0.25 μm×0.25 mm) after acetylation. The remaining products were quantified by HPLC (Shimadzu LC-20AB) attached with a refractive index (RI, Shimadzu RID 10A)

detector and an Aminex HPX-87H column (Bio-Rad, 300×7.8 mm). An aqueous mobile phase containing sulphuric acid (0.005 M) was used at a flow rate of 0.7 mL·min^{-1}. The column temperature was maintained at 65 °C throughout the analysis procedure. The cellulose conversion was calculated by measuring the weight of the solid before and after the reaction. The product yields were calculated by comparing the moles of carbon in the products by the moles of carbon in the starting quantity of cellulose.

Acknowledgements

We gratefully acknowledge the financial support provided by the National Program on Key Research Project (2016YFA0602900), National Natural Science Foundation of China (21473179 and 21273222), the Youth Innovation Promotion Association of Chinese Acamedy of Sciences (2014203), International Cooperation Project of Jilin Province (20170414012GH), Chinese Scholarship Council (201704910505), Chinese Academy of Science, and Cardiff Catalysis Institute, Cardiff University.

Keywords: Hierarchical carbon • macroporous carbon • nickel nanoparticles • cellulose • polyols

1. D. L. Klass, *Encyclopedia of Energy*, 1998, **Volume 1**.
2. J. C. Serrano-Ruiz and J. A. Dumesic, *Energy Environ. Sci*, 2011, **4**, 83-99.
3. C. H. Zhou, X. Xia, C. X. Lin, D. S. Tong and J. Beltramini, *Chem. Soc. Rev.*, 2011, **40**, 5588-5617.
4. Y. Wang, H. Song, L. Peng, Q. Zhang and S. Yao, *Biotechnol. Biotechnol. Equip*, 2014, **28**, 981-988.
5. H. Kobayashi, Y. Ito, T. Komanoya, Y. Hosaka, P. L. Dhepe, K. Kasai, K. Hara and A. Fukuoka, *Green Chem.*, 2011, **13**, 326-333.
6. A. Onda, T. Ochi and K. Yanagisawa, *Top. Catal.*, 2009, **52**, 801-807.
7. L. S. Ribeiro, J. J. Delgado, J. J. M. Orfao and M. F. R. Pereira, *Applied Catalysis B-Environmental*, 2017, **217**, 265-274.
8. W. P. Deng, M. Liu, X. S. Tan, Q. H. Zhang and Y. Wang, *J. Catal.*, 2010, **271**, 22-32.
9. A. Shrotri, H. Kobayashi, H. Kaiki, M. Yabushita and A. Fukuoka, *Ind. Eng. Chem. Res.*, 2017, **56**, 14471-14478.
10. S. Van de Vyver, J. Geboers, M. Dusselier, H. Schepers, T. Vosch, L. A. Zhang, G. Van Tendeloo, P. A. Jacobs and B. F. Sels, *ChemSusChem*, 2010, **3**, 698-701.
11. P. A. Lazaridis, S. A. Karakoulia, C. Teodorescu, N. Apostol, D. Macovei, A. Panteli, A. Delimitis, S. M. Coman, V. I. Parvulescu and K. S. Triantafyllidis, *Appl. Catal. B-Environ.*, 2017, **214**, 1-14.
12. J. Geboers, S. Van de Vyver, K. Carpentier, K. de Blochouse, P. Jacobs and B. Sels, *Chem. Commun.*, 2010, **46**, 3577-3579.
13. S. Van de Vyver, L. Peng, J. Geboers, H. Schepers, F. de Clippel, C. J. Gommes, B. Goderis, P. A. Jacobs and B. F. Sels, *Green Chem.*, 2010, **12**, 1560-1563.
14. J. F. Pang, A. Q. Wang, M. Y. Zheng and T. Zhang, *Chem. Commun.*, 2010, **46**, 6935-6937.
15. S. Suganuma, K. Nakajima, M. Kitano, D. Yamaguchi, H. Kato, S. Hayashi and M. Hara, *J. Am. Chem. Soc.*, 2008, **130**, 12787-12793.
16. H. Kobayashi, T. Komanoya, K. Hara and A. Fukuoka, *ChemSusChem*, 2010, **3**, 440-443.
17. Y. H. Zhang, A. Q. Wang and T. Zhang, *Chem. Commun.*, 2010, **46**, 862-864.
18. J. Pang, A. Wang, M. Zheng, Y. Zhang, Y. Huang, X. Chen and T. Zhang, *Green Chem.*, 2012, **14**, 614-617.
19. B. Zhang, X. Li, Q. Wu, C. Zhang, Y. Yu, M. Lan, X. Wei, Z. Ying, T. Liu, G. Liang and F. Zhao, *Green Chem.*, 2016, **18**, 3315-3323.
20. L. Liu, U. Díaz, R. Arenal, G. Agostini, P. Concepción and A. Corma, in *Nat. Mater.*, 2017, vol. 16, pp. 132-138.
21. G. Liang, H. Cheng, W. Li, L. He, Y. Yu and F. Zhao, *Green Chem.*, 2012, **14**, 2146-2149.
22. Y.-B. Huang and Y. Fu, *Green Chem.*, 2013, **15**, 1095-1111.
23. I. G. Baek, S. J. You and E. D. Park, *Bioresour. Technol.*, 2012, **114**, 684-690.
24. X. C. Guo, H. H. Dong, B. Li, L. L. Dong, X. D. Mu and X. F. Chen, *J Mol Catal A-Chem.*, 2017, **426**, 79-87.
25. O. V. Manaenkov, J. J. Mann, O. V. Kislitza, Y. Losovyj, B. D. Stein, D. G. Morgan, M. Pink, O. L. Lependina, Z. B. Shifrina, V. G. Matveeva, E. M. Sulman and L. M. Bronstein, *ACS Appl. Mater. Interfaces*, 2016, **8**, 21285-21293.
26. G. W. Huber, R. D. Cortright and J. A. Dumesic, *Angew. Chem. Int. Ed.*, 2004, **43**, 1549-1551.
27. T.-W. Kim, H.-D. Kim, K.-E. Jeong, H.-J. Chae, S.-Y. Jeong, C.-H. Lee and C.-U. Kim, *Green Chem.*, 2011, **13**, 1718-1728.
28. L. Negahdar, J. U. Oltmanns, S. Palkovits and R. Palkovits, *Appl. Catal. B-Environ.*, 2014, **147**, 677-683.
29. F. Shen, T. M. Guo, C. X. Bai, M. Qiu and X. H. Qi, *Fuel Process. Technol.*, 2018, **169**, 244-247.
30. A. T. To, P. W. Chung and A. Katz, *Angew. Chem. Int. Ed.*, 2015, **54**, 11050-11053.
31. A. Tiwari and M. Syväjärvi, *Advanced 2D Materials*, Scrivener Publishing, Canada, 2016.
32. J. Dhainaut, J.-P. Dacquin, A. F. Lee and K. Wilson, *Green Chem.*, 2010, **12**, 296-303.
33. S. Vaudreuil, M. Bousmina, S. Kaliaguine and L. Bonneviot, *Adv. Mater.*, 2001, **13**, 1310-1312.
34. D. Zhao, J. Feng, Q. Huo, N. Melosh, G. H. Fredrickson, B. F. Chmelka and G. D. Stucky, *Science*, 1998, **279**, 548-552.
35. S. Jun, S. H. Joo, R. Ryoo, M. Kruk, M. Jaroniec, Z. Liu, T. Ohsuna and O. Terasaki, *J. Am. Chem. Soc.*, 2000, **122**, 10712-10713.
36. G. Liang, L. He, H. Cheng, C. Zhang, X. Li, S.-i. Fujita, B. Zhang, M. Arai and F. Zhao, *J. Catal.*, 2015, **325**, 79-86.
37. S. L. Goertzen, K. D. Thériault, A. M. Oickle, A. C. Tarasuk and H. A. Andreas, *Carbon*, 2010, **48**, 1252-1261.
38. G. Liang, L. He, H. Cheng, W. Li, X. Li, C. Zhang, Y. Yu and F. Zhao, *J. Catal.*, 2014, **309**, 468-476.